J Mater Sci (2015) 50:6898–6906
DOI 10.1007/s10853-015-9228-1

Effect of Mg on the dielectric and electrical properties of $BaTiO_3$-based ceramics

Huiling Gong[1] · Xiaohui Wang[1] · Qiancheng Zhao[1] · Longtu Li[1]

Received: 8 May 2015 / Accepted: 1 July 2015 / Published online: 23 July 2015

Abstract $BaTiO_3$-based dielectric ceramics with grain sizes of 100–120 nm were prepared by the chemical coating approach and are promising for the application of ultrathin multilayer ceramic capacitors. The doping effects of Mg on the microstructures and dielectric properties of the $BaTiO_3$-based ceramics were investigated. The addition of Mg was beneficial for inhibiting the grain growth and improving sintering characteristics and improving the dielectric properties and reliability of the nano-$BaTiO_3$-based ceramics. The highly accelerated lifetime test and thermally stimulated depolarization current were employed to study the resistance degradation and conduction mechanism of the Mg-doped $BaTiO_3$ ceramics. It was determined that the reliability characteristics greatly depended on the Mg content. The addition of 2 mol% Mg was suitable for improving the reliability of the nano-$BaTiO_3$-based ceramics, which is an important parameter for the application of multilayer ceramic capacitors. However, further increasing the addition amount of Mg decreased the performance of the $BaTiO_3$-based ceramics.

✉ Xiaohui Wang
wxh@tsinghua.edu.cn

✉ Longtu Li
llt-dms@mail.tsinghua.edu.cn

Huiling Gong
gonghl10@mails.tsinghua.edu.cn

[1] State Key Lab of New Ceramics and Fine Processing, School of Materials Science and Engineering, Tsinghua University, Beijing 100084, China

Introduction

Multilayer ceramic capacitors used as passive components are in high demand, driven by the surface mounting technology and portable device markets. At present, the development trends of MLCCs are high capacity, miniaturization, low cost, high reliability and high-temperature stability [1, 2]. To achieve continuous cost-effectiveness of MLCCs, the base metal Ni electrode is considered to be a promising substitute for the precious Pd–Ag electrode. However, the base metal electrode MLCC (BME-MLCC) green pieces must be sintered in a reducing atmosphere to prevent the oxidation of the Ni electrodes, which will inevitably introduce many oxygen vacancies ($V_O^{\bullet\bullet}$) and free electrons [3, 4], which can lead to the degradation of the insulation resistance.

Avoiding the degradation of the insulation resistance has necessitated compositional modifications. The effects of doping with various oxides, especially the amphoteric rare-earth oxides (e.g. Ho^{3+} and Y^{3+}), have been extensively studied by many researchers. It has been determined that the doping of trivalent rare-earth ions and manganese ions is effective in improving the reliability of $BaTiO_3$ dielectrics [5–7]. Hence, the addition of a donor or an acceptor and the re-oxidation processes became the effective means of preventing the degradation of insulation resistance and to extend the service life of MLCCs [4, 8]. Among these processes, the incorporation of Mg acceptors into $BaTiO_3$ has the effect of fixing the positively charged oxygen vacancies through ionic compensation. This compensation suppresses electron generation and improves the insulation resistance. However, these oxygen vacancies generated by the incorporation of acceptor dopants are highly mobile at moderate temperatures and high electric fields, resulting in

time-dependent resistance degradation and reliability problems of the dielectric layers, as follows.

$$MgO \xrightarrow{TiO_2} Mg''_{Ti} + V_O^{\bullet\bullet} + O_O. \quad (1)$$

The doping effect of Mg has been intensively studied by Yoon et al. [9–16], including the resistance degradation behaviour, impedance spectra and thermally stimulated depolarization current in acceptor Mg-doped $BaTiO_3$. The behaviour of the resistance degradation indicated that the degradation rates increased with increasing acceptor Mg concentration in both the coarse and fine-grain specimens. The grain conductivity and the ionic transference number were associated with an increase in the oxygen vacancy concentration in the grain with the increase of the acceptor Mg concentration for the same grain size series. However, the grain size of the experimental samples is mainly concentrated in coarse-grained samples at the micron scale. As we know, to meet the requirements for MLCCs being smaller in size but providing large capacitance, the thickness of the dielectric layers should be $\sim$1 μm, and the grain sizes of $BaTiO_3$ ceramics should be approximately 100–200 nm or less to maintain sufficient reliability [17] and possess the so-called ''core–shell'' structure to meet the requirements for the temperature-stable characteristics of the capacitance for MLCCs [18, 19]. Furthermore, one of the most general directions for inhibiting resistance degradation is to decrease the grain size and thus increase the number of effective grain boundaries, which has a double Schottky barrier with higher potential energy and width to limit the transport of the oxygen vacancies across each boundary.

Therefore, researching the electrical and reliability characteristics is urgently important for acceptor (Mg)-doped nano-grained $BaTiO_3$-based ceramics in X7R-type ultrathin MLCCs applications. In this study, the X7R specification of the Electrical Industries Association (EIA) requires less than ±15 % change of the capacitance from the value at 25 °C in the range from −55 to 125 °C. In particular, as the grain size decreases, the formation of the "core–shell" structure becomes more difficult. To date, there are few papers examining the reliability and insulation resistance deterioration of MLCCs with ultra-fine-grain $BaTiO_3$ ceramic.

Thus, in the case of rare-earth and Mg co-doped nano-$BaTiO_3$-based systems, other than at the sub-micron scale, understanding the effect of the acceptor (Mg) on the dielectric properties and reliability is important for controlling the ceramic material formulation designed for ultrathin layer X7R-type Ni-MLCCs. In this paper, fine-grained X7R ceramics (100–120 nm) with a core–shell structure were obtained by the chemical coating method [20, 21] and sintered in reducing atmosphere. In particular, the effects of the acceptor (Mg) concentration on the microstructure, the dielectric properties and reliability of the ceramics have been investigated.

Experimental procedure

To induce core–shell structures in $BaTiO_3$-based ceramics, the $BaTiO_3$ powders were modified by a wet chemical coating approach, as described previously [20, 21]. The starting commercial $BaTiO_3$ powders (Samsung Electro-Mechanics Co. Ltd., Korea) with an average grain size of 80 nm ($c/a = 1.0095$) were ball milled in isopropanol for 16 h to obtain the well-dispersed $BaTiO_3$ suspending slurry. Next, the inorganic solution and organic solutions containing the additive elements were added into the slurry to improve the dielectric properties of the $BaTiO_3$ ceramics. For the preparation of the inorganic solution, water-soluble metal salts, including $Mn(CH_3COO)_2$ (99.8 %, Beijing Finechemical Co. Ltd., Beijing, China), 0.3 mol%; $Mg(NO_3)_2$ (99.8 %, Beijing Finechemical Co. Ltd., Beijing, China), 0–6 mol%; $Ca(NO_3)_2$ (99.8 %, Beijing Finechemical Co. Ltd., Beijing, China), 0.8 mol%; $Ho(NO_3)_3$ (99 %, Rare-chem Hi-tech Co. Ltd., Beijing, China), 0.5 mol%; and $Y(NO_3)_3$ (99 %, Rare-chem Hi-tech Co. Ltd., Beijing, China), 0.4 mol%, were dissolved in deionized water. For the organic solution, 1.5 mol% tetraethylorthosilicate (TEOS, $SiO_2 \geq 28.0$ %, Beijing Finechemical Co. Ltd., Beijing, China) was dissolved in a mixed solution of ethanol and deionized water (ethanol:water = 3:1, by volume). The molar ratios of these metal salts are relative to the molar content of $BaTiO_3$. Ammonia solution was then added to adjust the pH value of the mixed slurry to 9.5 for the sufficient precipitation of the additive elements, according to heterogeneous precipitation reactions (2) and (3):

$$M^{n+} + nNH_3 \cdot H_2O \rightarrow M(OH)_n \downarrow + nNH_4^+ \quad (2)$$

$$Si(OC_2H_5)_4 + 4H_2O \rightarrow Si(OH)_4 \downarrow + 4C_2H_5OH. \quad (3)$$

When the co-precipitation process ceased, the slurry was dried and calcined at 450 °C for 2 h, and the coated $BaTiO_3$ powders were finally obtained.

The coated powders were added with poly vinyl alcohol (PVA) binders and pressed into discs 10 mm in diameter at 2 MPa. The pellets were subsequently sintered in a reducing atmosphere ($H_2/N_2/H_2O$, $P_{O_2} = 10^{-13}$ atm) by a conventional sintering method ($T = 1210$ °C for 2 h followed by annealing in a weak oxidizing atmosphere at $T_{reo} = 1050$ °C for 150 min).

The microstructures of the ceramics were characterized by scanning electron microscopy (SEM, Leo-1530, Oberkochen, Germany). The temperature dependence of the dielectric constant and dielectric loss was measured

from −60 to 150 °C (heating rate 2 °C/min) at 1 kHz and an oscillation level of 1 Vrms using an impedance analyser (Model HP4192A, Hewlett-Packard Company, Santa Clara, California, USA) with a thermostat. The insulation resistance (IR) of the samples was measured by a pA meter (Model HP4140B, Hewlett-Packard Company, Santa Clara, California, USA). The thermally stimulated depolarization currents (TSDC) of the specimens were measured using an electrometer/high resistance meter (KEITHLEY 6517B; Keithley Instruments, Inc., Cleveland, OH, USA). Temperature data were collected by the quatro temperature controller of Novocontrol Technologies (Montabaur, Germany). The specimens were initially heated to a polarization temperature (T_p) in the range of 150–325 °C. A DC electric field (E_p) was also applied on the specimen for polarization, and E_p was chosen at 270 V/mm. The polarization was maintained for 10 min under a polarization temperature and DC polarization field. The specimen was then rapidly cooled to an initial temperature of −100 °C to freeze the polarized defects, while the dc polarization field was still maintained as the temperature decreased. By removing the E_p, the electrodes were short-circuited for 10 min to depolarize. Thereafter, the sample was heated with a heating rate (HR) of 5 °C/min to record the depolarization currents. The experimental artefact in the system indicates that the DC polarization electric field is defined as the positive direction. Therefore, the depolarization currents were negative, and the depolarizing current with changes in the temperature curve is the TSDC spectrum.

Results and discussion

The samples with different Mg contents were named Mg-1 (Mg = 0 mol%), Mg-2 (Mg = 1 mol%), Mg-3 (Mg = 2 mol%), Mg-4 (Mg = 4 mol%) and Mg-5 (Mg = 6 mol%).

Microstructures

Microstructures for the $BaTiO_3$-based ceramic samples doped with different acceptor Mg concentrations are shown in Fig. 1. A rapid grain growth was observed in the Mg-free sample Mg-1, with an average grain size of 1.03 μm, deteriorating the uniformity of the ceramics. When the doping content of Mg increased, the grain growth was inhibited to a certain extent in sample Mg-2, with highly non-uniform grain distributions, and the average grain size was 0.28 μm. When the Mg doping content further increased, as for samples Mg-3, Mg-4 and Mg-5, the average grain sizes (100–120 nm) were smaller, and the distributions were narrower and more uniform than for samples Mg-1 and Mg-2. In addition, with increasing Mg content, the shrinkage percent of the sample increased, as shown in Table 1. That is, Mg doping can affect the sintering properties. Within a certain range, increasing the Mg content can help promote the mass transfer of $BaTiO_3$ and improve the density of the ceramics. Mg doping is useful in promoting the sintering properties, and Mg can be the optional sintering aid in preparing the $BaTiO_3$-based ceramic capacitors.

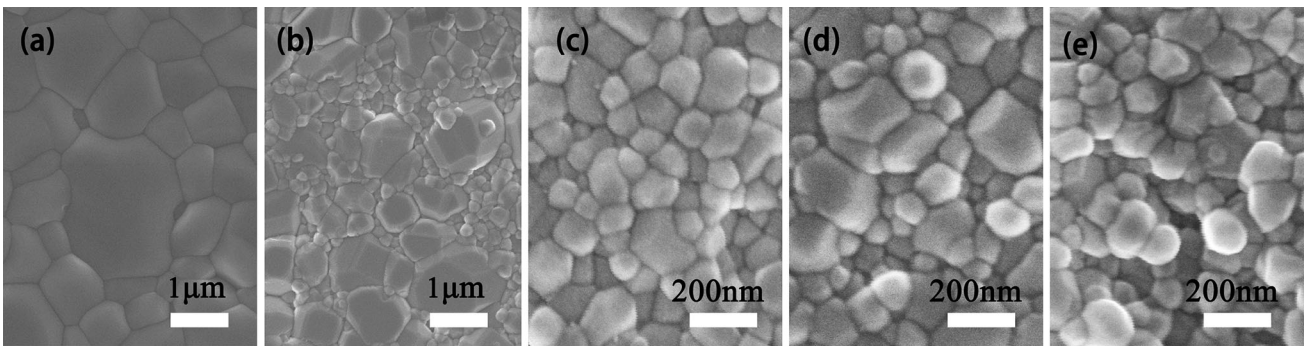

Fig. 1 The microstructures of the $BaTiO_3$-based ceramic samples with various Mg contents; **a** Mg-1; **b** Mg-2; **c** Mg-3; **d** Mg-4; **e** Mg-5

Table 1 Compositions and properties of the $BaTiO_3$-based ceramic samples with various Mg contents at room temperature

Sample	Mg content (mol%)	Shrinkage (%)	Dielectric constant	Loss	Resistivity (10^{12} Ω cm)
Mg-1	0	13.97	1046	0.0131	0.26
Mg-2	1	16.33	1591	0.0105	3.46
Mg-3	2	16.93	2454	0.0053	1.73
Mg-4	4	17.17	2265	0.0061	1.67
Mg-5	6	18.07	2098	0.0075	1.65

Figure 2 shows a set of XRD patterns of samples doped with various amounts of Mg. All patterns show a desired single perovskite phase, referring to $BaTiO_3$, and no secondary phase was detected. However, the split in the XRD peaks is more evident for samples Mg-1 and Mg-2 with a larger grain size.

Dielectric response

The temperature dependence of the dielectric properties (K–T curve) and the capacitance change based on the capacitance at 25 °C (TCC curve) are described in Fig. 3. There were sharp dielectric peaks for samples Mg-1 and Mg-2. This signified that the core–shell structures did not form perfectly, and the abnormal grain growth led to the deterioration of the dielectric properties (lower dielectric constant at room temperature, higher dielectric loss and worse temperature stability) in the samples with both normal and lower Mg content, as described in Table 1.

It was demonstrated by research in the literature that the Mg ions play an important role in the formation of the core–shell structure in the BT-MgO-Ho_2O_3-based system, and an appropriate amount of Mg was necessary for suppressing the diffusion of Ho into the core [22]. Thus, for sample Mg-1 without Mg and Mg-2 with a lower Mg content, it is difficult for them to form a core–shell structure, and the solid-state solution formed. For the three other samples, Mg-3, Mg-4 and Mg-5, with a higher content of Mg, the curves for the temperature dependence of the dielectric properties are flat, all meeting the X7R specification, indicating that the doping of the appropriate Mg content is conducive to forming the "core–shell" structure for improving the temperature stability of dielectric ceramics. Additionally, the other three samples possess a higher dielectric constant and lower dielectric loss (less than 1 %), and as the Mg doping amount increases, the dielectric constant is reduced, as described in Table 1.

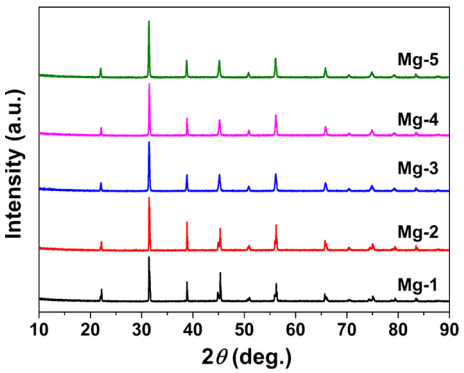

Fig. 2 XRD patterns of the $BaTiO_3$-based ceramic samples doped with various amounts of Mg

Electrical properties

The insulation resistivity at room temperature for samples with different Mg doping contents is shown in Table 1. The insulation resistivity of the Mg-free sample is the lowest because this sample has the largest average grain size. The insulation resistivity of sample Mg-2 is the largest, which may be related to the reduction of the average grain size compared with Mg-1 and the lower acceptor doping concentration compared with the other three samples. The insulation resistivity of samples Mg-3, Mg-4 and Mg-5 are very similar because of the similar grain size compared with samples Mg-1 and Mg-2. The small differences in the insulation resistivity for the three samples may be caused by the acceptor doping concentration, but the insulation resistivity at room temperature seems to be insensitive to the acceptor doping concentration in the nano-grained samples.

It is well known that the oxygen vacancies generated by the incorporation of acceptor dopants (Mg) are highly mobile at moderate temperatures and under high electric fields in the dielectrics, which causes a time-dependent resistance degradation and reliability problems. Thus, the time dependence of the insulation resistance of the $BaTiO_3$-based ceramic samples at a high temperature (260 °C) under a direct current (DC) field of 1200 V/mm was investigated. The highly accelerated lifetime test

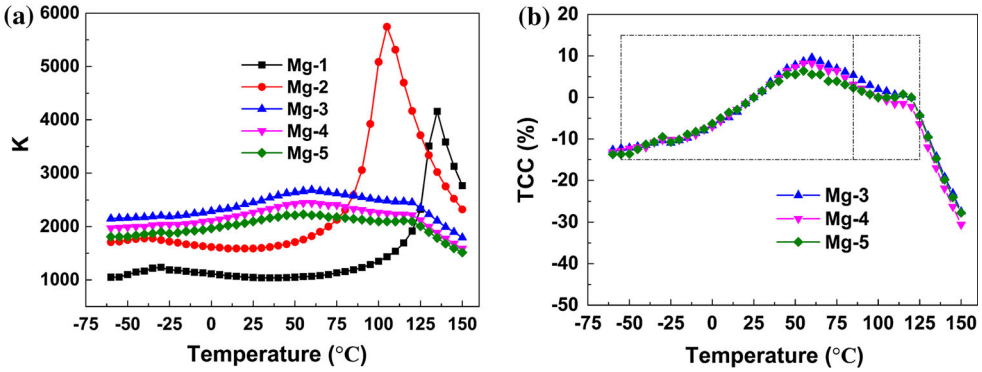

Fig. 3 Temperature dependence of **a** the dielectric constant and **b** the temperature coefficient of capacitance

(HALT) was repeated several times to exclude data error. The resistivity decreases at first and remains at a certain value for an extended period of time. It was found that the behaviours of the insulation resistivity for samples were highly different from that at room temperature, and the reliability characteristics greatly depended on the Mg-doped content. As seen in Fig. 4, the insulation resistivity of sample Mg-1 is always the highest, and the insulation resistivity of sample Mg-2 is the second highest. As time went by, there was no obvious tendency of the resistivity to decrease.

At the beginning, the insulation resistivity of samples Mg-3, Mg-4 and Mg-5 was highly similar to one another and was the same as the results observed at room temperature. However, the electrical properties of sample Mg-5 started to deteriorate after 30 h, and the insulation resistivity instantly dropped to below 10^9 Ω cm. Many studies have examined the degradation mechanisms of the dielectric materials [4, 23–25]. It is generally agreed that the insulation resistance degradation of dielectric ceramics under simultaneous temperature and DC electrical field stresses is caused by the electromigration of oxygen vacancies towards the cathode due to their positive charge with respect to the regular lattice. Sample Mg-5, with its high acceptor concentration, produced more oxygen vacancies and broke down quickly. With testing time of 80 h, the insulation resistance of the sample Mg-4 began to slowly decrease and the reduce rate began to increase after 95 h. However, there was no tendency to reduce the insulation resistivity for sample Mg-3.

To investigate further the effect of acceptor Mg doping on the insulation resistance degradation behaviour, the thermally stimulated depolarization current (TSDC) measurement was adopted to identify the type of defects, such as defect dipoles, trap charges, and space charges, and determine the resistance degradation mechanism.

Figure 5 shows the TSDC measurement results of the Mg-doped $BaTiO_3$-based ceramics with various polarization

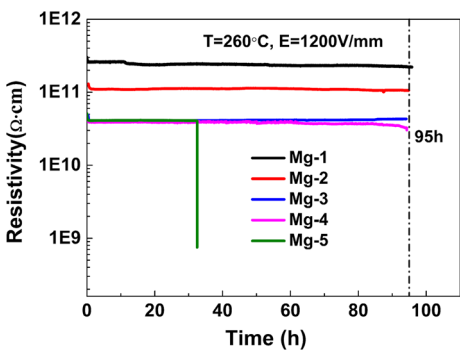

Fig. 4 Resistivity versus time of the $BaTiO_3$-based ceramics measured at an elevated temperature of 260 °C and a DC bias of 1200 V/mm

temperatures (150–325 °C) and a fixed DC polarization field of 270 V/mm. The polarization time is 10 min, and the heating rate is 5 °C/min. As shown in Fig. 5a, b, the spectra were dominated by the release of pyroelectric current around the phase transition temperatures of $BaTiO_3$ for samples Mg-1 and Mg-2. A second pyroelectric current peak (pyro peak) was generated because of the ferroelectric–paraelectric phase transition, and the peak position approximately corresponded to the results of the K–T curves. After further increasing the Mg content, the TSDC spectra showed significant changes. Thus, the behaviours of the TSDC could be influenced by the acceptor Mg content.

It is well known that the microstructure of X7R $BaTiO_3$-based ceramics often contains core–shell structures. In the TSDC spectra of Ni-MLCCs, Morita et al. have assigned the low- and high-temperature peaks to the release of the pyroelectric current of the shell and the core, respectively [26]. In this study, in samples Mg-3, Mg-4 and Mg-5, the spectra are dominated by three pyroelectric peaks below 150 °C, and the pyroelectric peaks of the core and the shell suggest that the ferroelectric phase can still be present and polarized during the cooling steps. Above the Curie temperature, the spectra are dominated by the α peak, which may be related to defects with high activation temperatures and the associated activation energies, such as oxygen vacancies. The intensity of the α peak, which corresponds to the thermally stimulated depolarization current density, continues to increase with increasing polarization temperatures and the peak position, which corresponds to the relaxation peak temperature (T_m), and migrates to a higher temperature.

The maximum thermally stimulated depolarization current peak density (J_{max}) of α peak versus the polarization temperature (T_p) with different Mg contents is shown in Fig. 5f. The figure shows that the increase of the TSDC peak density (J_{max}) corresponds to higher T_p, indicating stronger polarization conditions in each specimen. For the same J_{max} condition, T_p decreases systematically with an increase of the Mg content. In other words, an increase of the Mg content results in an increase of J_{max} under the same polarization condition. Therefore, the defect concentration corresponding to the thermally stimulated depolarization current density increases with increasing Mg contents.

It can be observed in Fig. 5c, d and e that there is an increase of T_m, corresponding to an increase of J_{max}, by stronger polarization conditions, that is, higher T_P. Such behaviour is a typical characteristic of polarization because of space charge migration [27–29]. Thus, these TDSC peaks are supposed to be associated with the relaxation of oxygen vacancies after a spatial redistribution under the polarizing field.

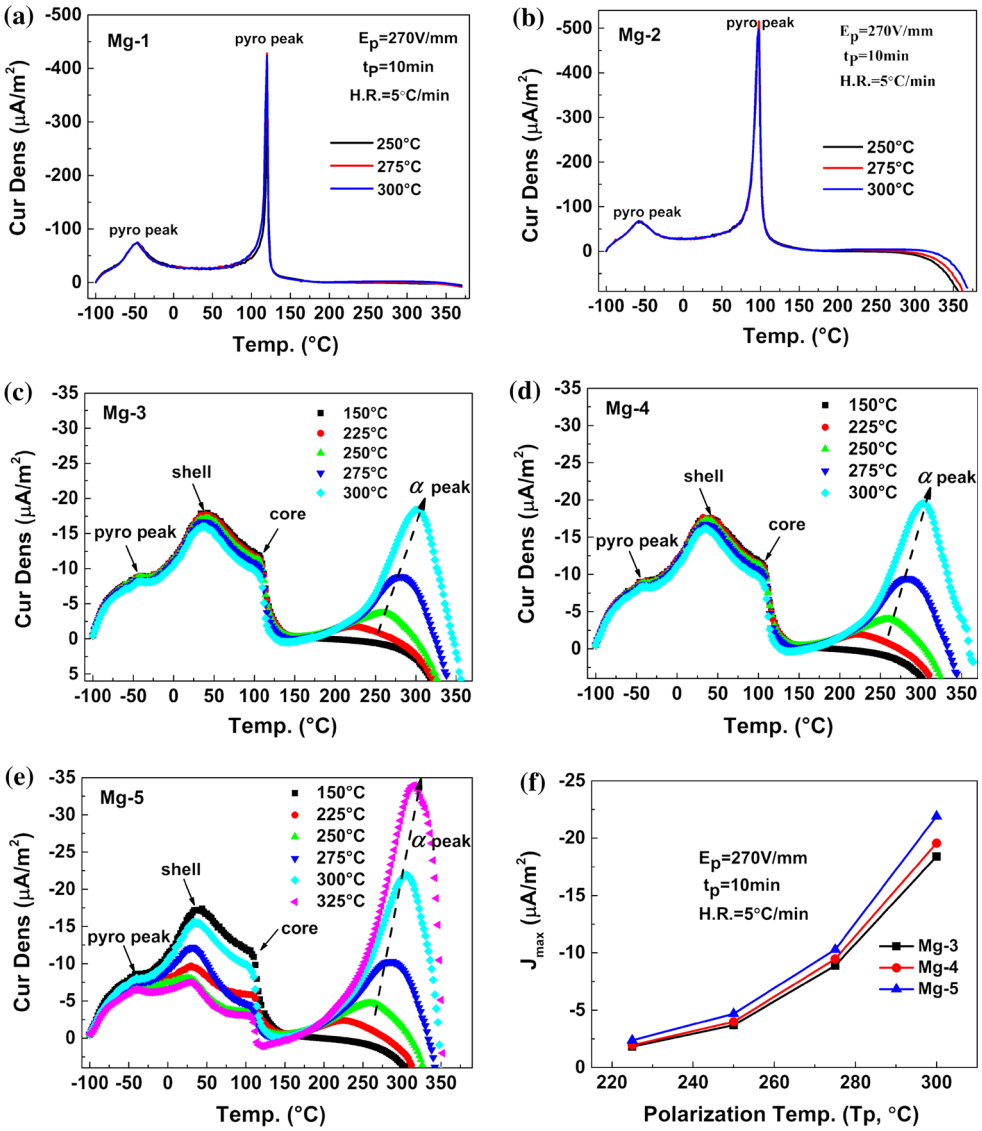

Fig. 5 Thermally stimulated depolarization current (TSDC) of the $BaTiO_3$-based samples **a** Mg-1, **b** Mg-2, **c** Mg-3, **d** Mg-4, **e** Mg-5, **f** comparison of the TSDC peaks changing with polarization temperatures for different acceptor Mg concentrations

The TSDC spectra for samples after HALT were also investigated. The TSDC spectra for sample Mg-1 were unchanged. As T_p reached 225 °C, the high-temperature α peak appeared for sample Mg-2, as shown in Fig. 6, and it increased with an increase of T_P from 225 to 250 °C. This finding is observed because certain defects were activated after HALT, and the TSDC peak could appear under a relatively weaker polarization condition, corresponding to a lower T_p.

For samples Mg-3, Mg-4 and Mg-5, after HALT, the spectra were almost unchanged, but the intensity of the α peak increased under the same polarization conditions. Figure 7 shows the comparison of the J_{max} before and after HALT with a polarization temperature of 275 °C. It can be observed that the J_{max} after HALT showed a systematic dependence on acceptor Mg concentrations. J_{max} increased for samples after HALT with different acceptor Mg concentrations, but J_{max} increased more heavily for samples with higher Mg concentrations.

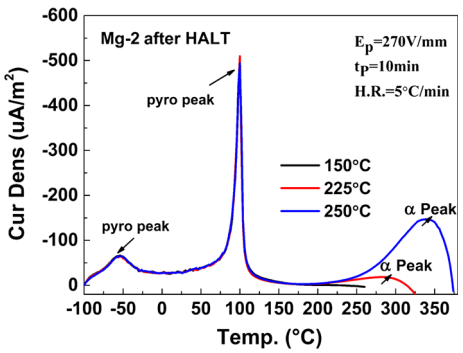

Fig. 6 Thermally stimulated depolarization current (TSDC) of the $BaTiO_3$-based sample Mg-2 after 95 h HALT

Thermally stimulated depolarization current with a single relaxation can be mathematically described by the following equation [10, 13, 30, 31].

$$J(T) = Cn_0 s \times \exp\left(-\frac{E}{kT}\right) \times \exp\left[-\frac{s}{a}\int_{T_0}^{T} \exp\left(-\frac{E}{kT}\right) dT\right]. \quad (4)$$

In Eq. (4), J is the current density, C is the geometry constant, s is a frequency factor that is related to the material vibrational frequency, a denotes the heating rate of measurement, n_0 is the concentration of trap charge carriers, E is the activation energy, k is the Boltzmann constant and T is the absolute temperature. Both sides of Eq. (2) vary with the natural logarithm, and the obtained equation may describe the peak region of the TSDC as a general curve, as shown in the following equation [32].

$$-\ln\left[\frac{J(T)}{\text{Const.}}\right] = \frac{E}{kT} + \exp\left(\frac{E}{kT_m} - \frac{E}{kT}\right). \quad (5)$$

Here, T_m corresponds to the temperature of the current peak on the TSDC spectrum. The activation energy, E, which was associated with the relaxation process, can be derived by fitting measured TSDC data to the universal curve in Eq. (4).

Figure 8a shows the fitted activation energy E versus the polarization temperatures (T_p) for samples with different Mg contents. Specimens Mg-1 and Mg-2 only show the pyroelectric current peak, and thus, there is no corresponding activation energy. For samples Mg-3, Mg-4 and Mg-5, the activation energy values range from 0.75 to 0.94 eV. These values of the activation energy of the oxygen vacancy relaxation are roughly similar to the literature data of titanate ceramics, where the values range from 0.86 to 1.03 eV [28–30, 33]. According to the movement characteristics of the relaxation peaks and the activation energy values, these TSDC relaxation peaks are considered to be from the space charge polarization due to mobile oxygen vacancies. Contrary to the result of the invariant values of approximately 0.9 eV, which is irrespective of the Mg concentration [13], the activation energy decreased with increasing acceptor (Mg) concentration at the same polarization temperature. It is likely that the oxygen vacancy concentration in the specimen showed a systematic dependence on the acceptor Mg concentration in a relative broader acceptor Mg concentration range. Thus, the activation energy decreased with increasing acceptor (Mg) concentration.

The activation energy E for samples after HALT was also fitted, and the fitted activation energy E versus the polarization temperatures (T_p) for samples with different Mg contents is shown in Fig. 8b. After degradation, the activation energy of all samples decreased with a different amplitude at the same polarization temperature. The activation energy values range from 0.56 to 0.93 eV, and the variation amount of the activation energy for sample Mg-5 was the largest. This result indicates that the defect concentrations increased in sample Mg-5, and the defects are more likely to be polarized after HALT, corresponding to an increase of the thermally stimulated depolarization current, as mentioned above. Thus, the behaviour of a fast resistance degradation process with an increase of the Mg concentration observed in the HALT part is directly associated with an increase of J_{max} and a decrease of the activation energy E in TSDC, which corresponds to an increase of the oxygen vacancy concentration.

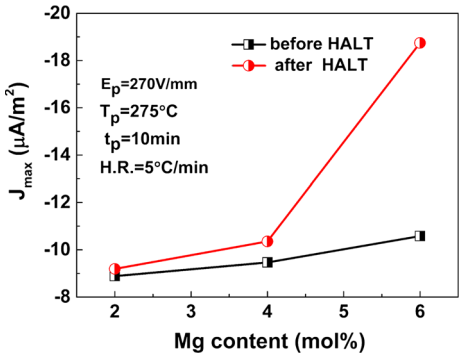

Fig. 7 Comparison of the TSDC peaks changing with acceptor Mg concentrations for samples before and after HALT

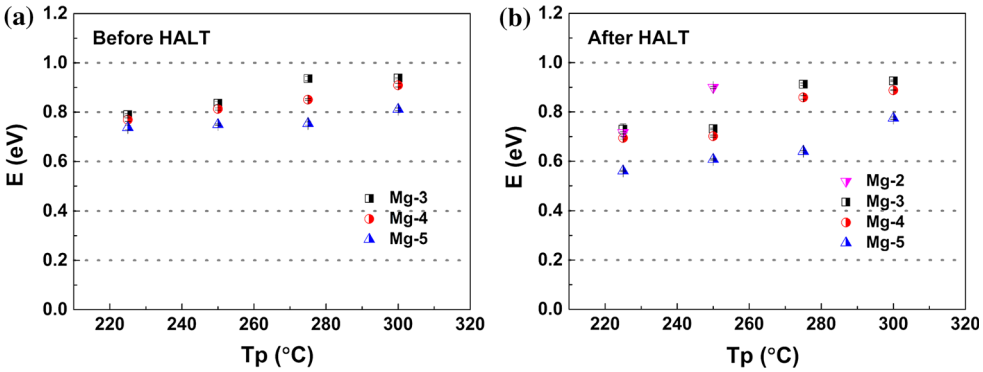

Fig. 8 Activation energy E versus polarization temperature (T_p) for samples with different acceptor Mg concentrations **a** before HALT and **b** after HALT

Conclusions

Nano-grained $BaTiO_3$-based dielectric ceramics (100–120 nm) with core–shell structures were prepared by the chemical coating approach. The microstructures and the reliability characteristics strongly depended on the Mg doping content in the $BaTiO_3$ ceramics. The addition of Mg is beneficial for inhibiting grain growth and improving the sintering characteristics. The sample with a high acceptor concentration of 6 mol%, producing more oxygen vacancies, degrades quickly, and an appropriate amount of 2 mol% Mg in nano-$BaTiO_3$-based ceramics was beneficial for improving the reliability. The results of the TSDC spectra also indicate that the defect concentration increases with the increasing of Mg contents. The behaviour of a fast resistance degradation process with an increase of the Mg concentration is directly associated with an increase of J_{max} and a decrease of the activation energy E in TSDC, which corresponds to an increase of the oxygen vacancy concentration. The results of this experiment are significant for designing the ceramic material formulation designed for ultrathin layer Ni-MLCCs.

Acknowledgements The work was supported by the Ministry of Sciences and Technology of China through the National Basic Research Program of China (973 Program 2015CB654604), the National Natural Science Foundation of China for Creative Research Groups (Grant No. 51221291) and the National Natural Science Foundation of China (Grant No. 51272123) and was also supported by CBMI Construction Co., Ltd.

References

1. Pan M-J, Randall CA (2010) A brief introduction to ceramic capacitors. IEEE Electr Insul Mag 26:44–50
2. Kishi H, Mizuno Y, Chazono H (2003) Base-metal electrode-multilayer ceramic capacitors: past, present and future perspectives. Jpn J Appl Phys 42:1–15
3. Woodward DI, Reaney IM, Yang GY, Dickey EC, Randall CA (2004) Vacancy ordering in reduced barium titanate. Appl Phys Lett 84:4650–4652
4. Yamamatsu J, Kawano N, Arashi T, Sato A, Nakano Y, Nomura T (1996) Reliability of multilayer ceramic capacitors with nickel electrodes. J Power Sources 60:199–203
5. Mitic VV, Nikolic ZS, Pavlovic VB, Paunovic V, Miljkovic M, Jordovic B, Zivkovic L (2010) Influence of rare-earth dopants on barium titanate ceramics microstructure and corresponding electrical properties. J Am Ceram Soc 93:132–137
6. Kang D, Park T, Kim J, Kim J, Lee H, Cho H (2010) Effect of dysprosium oxide addition on the microstructure and dielectric properties of $BaTiO_3$ ceramics. Electron Mater Lett 6:145–149
7. Gong HL, Wang XH, Zhang SP, Tian ZB, Li LT (2012) Electrical and reliability characteristics of Mn-doped nano $BaTiO_3$-based ceramics for ultrathin multilayer ceramic capacitor application. J Appl Phys 112:114119-1–114119-6
8. Kaneda K, Lee S, Donnelly NJ, Qu W, Randall CA, Mizuno Y (2011) Kinetics of oxygen diffusion into multilayer ceramic capacitors during the re-oxidation process and its implications on dielectric properties. J Am Ceram Soc 94:3934–3940
9. Yoon S-H, Hong M-H, Hong J-O, Kim Y-T, Hur K-H (2007) Effect of acceptor (Mg) concentration on the electrical resistance at room and high (200 °C) temperatures of acceptor (Mg)-doped BaTiO3 ceramics. J Appl Phys 102:054105-1–054105-9
10. Yoon S-H, Randall CA, Hur K-H (2010) Correlation between resistance degradation and thermally stimulated depolarization current in acceptor (Mg)-doped $BaTiO_3$ submicrometer fine-grain ceramics. J Am Ceram Soc 93:1950–1956
11. Yoon S-H, Randall CA, Hur K-H (2010) Effect of acceptor concentration on the bulk electrical conduction in acceptor (Mg)-doped $BaTiO_3$. J Appl Phys 107:103721-1–103721-8
12. Yoon S-H, Randall CA, Hur K-H (2010) Difference between resistance degradation of fixed valence acceptor (Mg) and variable valence acceptor (Mn)-doped $BaTiO_3$ ceramics. J Appl Phys 108:064101-1–064101-9
13. Yoon S-H, Randall CA, Hur K-H (2009) Effect of acceptor (Mg) concentration on the resistance degradation behavior in acceptor (Mg)-doped $BaTiO_3$ bulk ceramics: II. thermally stimulated depolarization current analysis. J Am Ceram Soc 92:1766–1772
14. Yoon S-H, Randall CA, Hur K-H (2009) Influence of grain size on impedance spectra and resistance degradation behavior in acceptor (Mg)-doped $BaTiO_3$ ceramics. J Am Ceram Soc 92:2944–2952
15. Yoon S-H, Kwon S-H, Hur K-H (2011) Dielectric relaxation behavior of acceptor (Mg)-doped $BaTiO_3$. J Appl Phys 109:084117-1–084117-8
16. Yoon S-H, Randall CA, Hur K-H (2009) Effect of acceptor (Mg) concentration on the resistance degradation Behavior in acceptor (Mg)-doped $BaTiO_3$ bulk ceramics: I. impedance analysis. J Am Ceram Soc 92:1758–1765
17. Yang GY, Dickey EC, Randall CA, Barber DE, Pinceloup P, Henderson MA, Hill RA, Beeson JJ, Skamser DJ (2004) Oxygen nonstoichiometry and dielectric evolution of $BaTiO_3$. Part I—improvement of insulation resistance with reoxidation. J Appl Phys 96:7492–7499
18. Park Y, Kim YH (1995) The dielectric temperature characteristic of additives modified barium-titanate having core-shell structured ceramics. J Mater Res 10:2770–2776
19. Hennings D, Rosenstein G (1984) Temperature-stable dielectrics based on chemically inhomogeneous $BaTiO_3$. J Am Ceram Soc 67:249–254
20. Tian Z, Wang X, Shu L, Wang T, Song T-H, Gui Z, Li L (2009) Preparation of nano $BaTiO_3$-based ceramics for multilayer ceramic capacitor application by chemical coating method. J Am Ceram Soc 92:830–833
21. Zhang Y, Wang X, Tian Z, Hur K-H, Li L (2011) Preparation of BME MLCC powders by aqueous chemical coating method. J Am Ceram Soc 94:3286–3290
22. Kishi H, Okino Y, Honda M, Iguchi Y, Imaeda M, Takahashi Y, Ohsato H, Okuda T (1997) The effect of MgO and rare-earth oxide on formation behavior of core-shell structure in $BaTiO_3$. Jpn J Appl Phys 36:5954–5957
23. Waser R, Baiatu T, Hardtl KH (1990) Dc electrical degradation of perovskite-type titanates. 1. ceramics. J Am Ceram Soc 73:1645–1653
24. Tsurumi T, Shono M, Kakemoto H, Wada S, Saito K, Chazono H (2005) Mechanism of capacitance aging under Dc electric fields in multilayer ceramic capacitors with X7R characteristics. Jpn J Appl Phys 44:6989–6994
25. Chazono H, Kishi H (2001) Dc-electrical degradation of the BT-based material for multilayer ceramic capacitor with Ni internal electrode: impedance analysis and microstructure. Jpn J Appl Phys 40:5624–5629
26. Morita K, Mizuno Y, Chazono H, Kishi H, Yang G-Y, Liu W-E, Dickey EC, Randall CA (2007) Electric conduction of thin-layer Ni-multilayer ceramic capacitors with core-shell structure $BaTiO_3$. Jpn J Appl Phys 46:2984–2990

27. Takeoka S, Morita K, Mizuno Y, Kishi H (2007) Thermally stimulated current (TSC) studies on resistance degradation of Ni-MLCC. Ferroelectrics 356:370–376
28. Sheng JX, Fukami T, Karasawa J (1998) X-ray photoemission spectroscopy (XPS) and thermally stimulated current (TSC) studies on the resistance degradation of iron-doped titania ceramics. J Am Ceram Soc 81:260–262
29. Hafid H, Takeoka S, Nishida S, Fukami T, Sheng J (1998) Dielectric and conduction properties in nickel doped barium strontium titanate ceramics. Jpn J Appl Phys 37:3370–3373
30. Liu W, Randall CA (2008) Thermally stimulated relaxation in Fe-doped $SrTiO_3$ systems: II. Degradation of $SrTiO_3$ dielectrics. J Am Ceram Soc 91:3251–3257
31. Lee H, Kim JR, Lanagan MJ, Trolier-McKinstry S, Randall CA (2013) High-energy density dielectrics and capacitors for elevated temperatures: Ca(Zr, Ti)O3. J Am Ceram Soc 96:1209–1213
32. Haering RR, Adams EN (1960) Theory and application of thermally stimulated currents in photoconductors. Phys Rev 117:451–454
33. Liu W, Randall CA (2008) Thermally stimulated relaxation in Fe-doped $SrTiO_3$ systems: I. Single crystals. J Am Ceram Soc 91:3245–3250